View Article Online
DOI: 10.1039/C7TC05009G

Journal Name

ARTICLE

Proton-conductive materials formed by coumarin photocrosslinked ionic liquid crystal dendrimers

Received 00th January 20xx,
Accepted 00th January 20xx

DOI: 10.1039/x0xx00000x

www.rsc.org/

Alberto Concellón,[a] Ting Liang,[b] Albertus P. H. J. Schenning,[b,c] José Luis Serrano,[d] Pilar Romero,*[a] and Mercedes Marcos*[a]

In this work, we have successfully examined for first time the use of ionic dendrimers as building blocks for the preparation of 1D and 2D proton conductive materials. For this purpose, a new family of liquid crystalline dendrimers have been synthesized by ionic self-assembly of poly(amidoamine) (PAMAM) dendrimers bearing 4, 8, 16, 32 or 64 NH_2 terminal groups and a coumarin-containing bifunctional dendron. The noncovalent architectures were obtained by the formation of the ionic salts between the carboxylic acid group of the dendron and the terminal amine groups of the PAMAM dendrimer. The liquid crystal properties have been investigated by polarized optical microscopy (POM), differential scanning calorimetry (DSC) and X-ray diffraction (XRD). All the compounds exhibited mesogenic behavior with smectic A or hexagonal columnar mesophases depending on the generation of the dendrimer. Coumarin photodimerization was used as crosslinking reaction to obtain liquid crystalline polymer networks. All the materials showed good proton conductive properties as the LC arrangement leads to the presence of ionic nanosegregated areas (formed by the ion pairs) that favor proton conduction.

Introduction

Ion transport is an important phenomenon in biological processes, batteries and separation technologies. The use of ionic liquid crystals (LCs) has been found to be a versatile approach for the development of ion transporting materials.[1-2] In fact, LC materials can self-organize into various nanostructured phases, such as nematic, smectic or columnar. These nanosegregated structures provide well-organized channels for the transport of electrons, holes or ions.[3-6] Columnar and smectic arrangements may lead to the formation of 1D and 2D channels (respectively) capable of transporting ions. As with all LC properties, ion transport is highly anisotropic thus, the orientation of the 1D and 2D channels on the macroscopic scale is an important and challenging feature. Smectic LCs can be considered as 2D ion conductors with ion conduction in the directions within the layer plane. However, LCs showing columnar mesophases can be used to create 1D ion conductors, with ion conduction taking place in the direction of the columnar axes.[7-8] Therefore, LC materials have potential as new functional electrolytes for electrochemical devices; for example, in lithium-ion batteries (transport of Li^+ ion), dye-sensitized solar cells (transport of the I^-/I_3^- redox couple) or fuel cells (proton transport).[9-18]

Nanostructured LC phases can be stabilized by photopolymerization to maintain the anisotropic ion transport over a longer period of time. Crosslinking of polymerizable LC monomers in their mesophase can yield nanostructured, thermally and mechanically stable membrane materials with permanent pathways for ion transport.[19-23]

Over the last few years, we have been working on LC dendrimers with the aim of combining the inherent properties of the dendrimer scaffold with the anisotropic properties provided by the LC state.[24-25] LC dendrimers are generally prepared by the introduction of promesogenic units at the periphery of a preformed dendrimer. However, it is possible the design of LC dendrimers without any promesogenic unit. Ionic LC dendrimers are the most interesting example, nanosegregation between polar and apolar regions was the driving force for the formation of the observed mesophases.[26-31] In addition, the structural versatility of dendrimers allows the introduction of different functional units on the periphery, obtaining materials with potential applications in targeted drug-delivery, optoelectronics, light harvesting and sensors.[32-35]

[a] Instituto de Ciencia de Materiales de Aragón, Departamento de Química Orgánica, Universidad de Zaragoza-CSIC, 50009, Zaragoza, Spain. Email: promero@unizar.es, mmarcos@unizar.es
[b] Department of Functional Organic Materials and Devices, Chemical Engineering and Chemistry, Eindhoven University of Technology, De Rondom 70, 5612 AP, Eindhoven, The Netherlands
[c] Institute for Complex Molecular Systems (ICMS), Eindhoven University of Technology, P. O. Box 513, 5600 MB, Eindhoven, The Netherlands.
[d] Instituto de Nanociencia de Aragón, Departamento de Química Orgánica, Universidad de Zaragoza, 50009, Zaragoza, Spain.

View Article Online
DOI: 10.1039/C7TC05009G

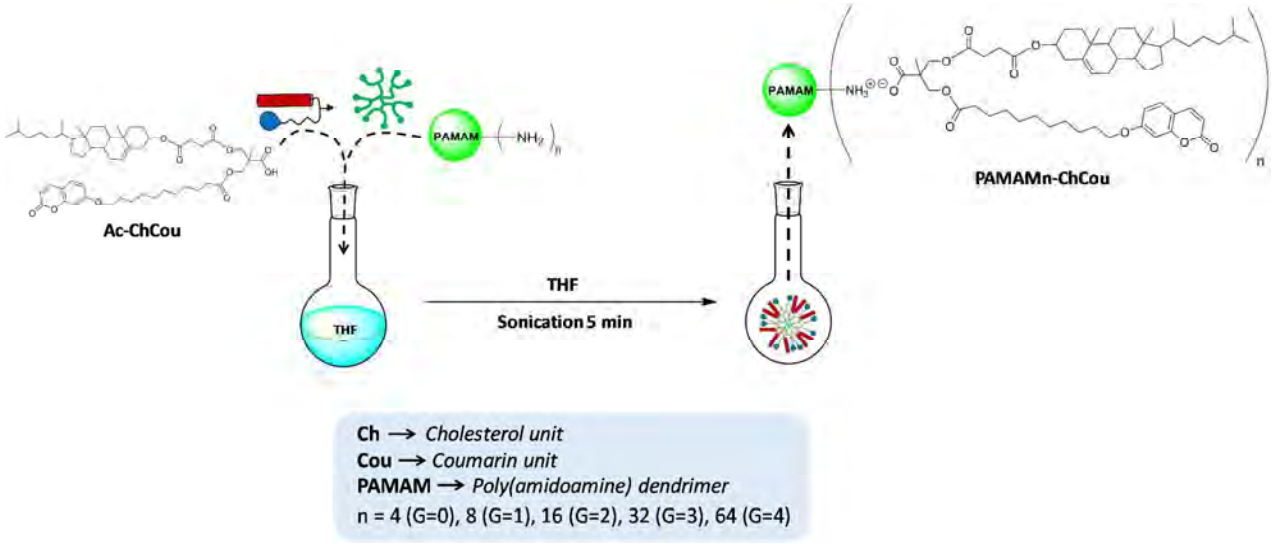

Figure 1. Schematic representation of the ionic self-assembly process to prepare the ionic LC dendrimers and the nomenclature of the ionic dendrimers.

To date, proton conductivity has been reported with low-molecular-weight mesogenic compounds that were stabilized by photocrosslinking to maintain the ionic conductivity over a longer period of time. In the present study, to develop 1D and 2D proton-conductive materials, we have examined the supramolecular LC organization of ionic dendrimers. A new family of ionic hybrid dendrimers were synthesized from poly(amidoamine) (PAMAM) dendrimer generations 0 to 4 (bearing 4, 8, 16, 32 or 64 NH_2 terminal groups) (**Figure 1**). PAMAM was surrounded by carboxylic acid dendrons bifunctionalized with a promesogenic unit (cholesteryl hemisuccinate) and coumarin moieties. Coumarin derivatives have been widely used as fluorophores in material science.[36-42] In this work coumarin was chosen as reactive group for the crosslinking reaction. Upon UV irradiation, coumarins undergo [2+2] cycloaddition to yield cyclobutane dimers. It doesn't require an initiator or catalyst and side reactions may be avoided.

Results and discussion

Synthesis and Characterization of Ionic dendrimers

The carboxylic acid dendron (**Ac-ChCou**, **Figure 1**) was prepared by the synthetic route and the experimental details given in the Supporting Information.

Ionic dendrimers were prepared by mixing a tetrahydrofuran (THF) solution of **Ac-ChCou** with a solution of the corresponding generation of PAMAM dendrimer in the stoichiometry necessary to functionalize all terminal amine groups. The mixture was ultrasonicated for 5 min, then the THF was slowly evaporated at room temperature and the sample was dried in vacuum at 40 °C until the weight remained constant. The formation of ionic interactions between the PAMAM dendrimer and the dendron acids was studied by infrared spectroscopy (IR) and by nuclear magnetic resonance (NMR).

As a representative example that demonstrates the formation of the ionic salts, the FTIR spectra of **Ac-ChCou**, **PAMAM16** and the corresponding ionic dendrimer is shown in **Figure 2**. In the spectrum of **Ac-ChCou**, three C=O stretching bands appeared at 1683, 1730 and 1741 cm^{-1}. The band at 1730 cm^{-1} is assigned to the ester groups, whereas the bands at 1686 and 1741 cm^{-1} correspond to the dimeric and free form of the carboxylic acid group, respectively. In the spectrum of **PAMAM16-ChCou** the signals at 1686 and 1741 were replaced by two new bands at around 1550 and 1400 cm^{-1} due to the asymmetric and symmetric stretching modes of the carboxylate group.

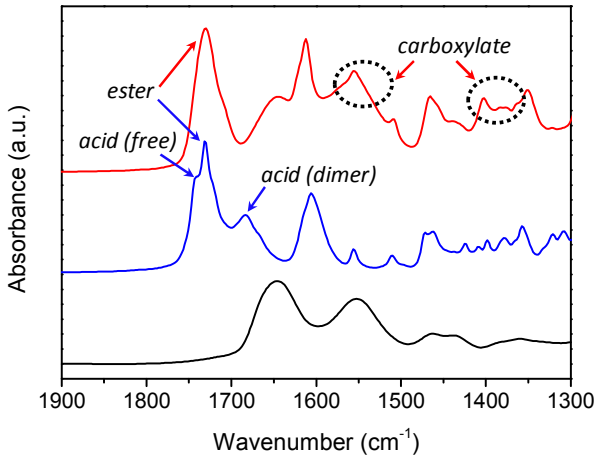

Figure 2. FTIR spectra (C=O st. region) of **PAMAM16** (black line), **Ac-ChCou** (blue line), and **PAMAM16-ChCou** (red line). (See **Figure S1** for the FTIR spectra in the complete frequency range)

View Article Online
DOI: 10.1039/C7TC05009G

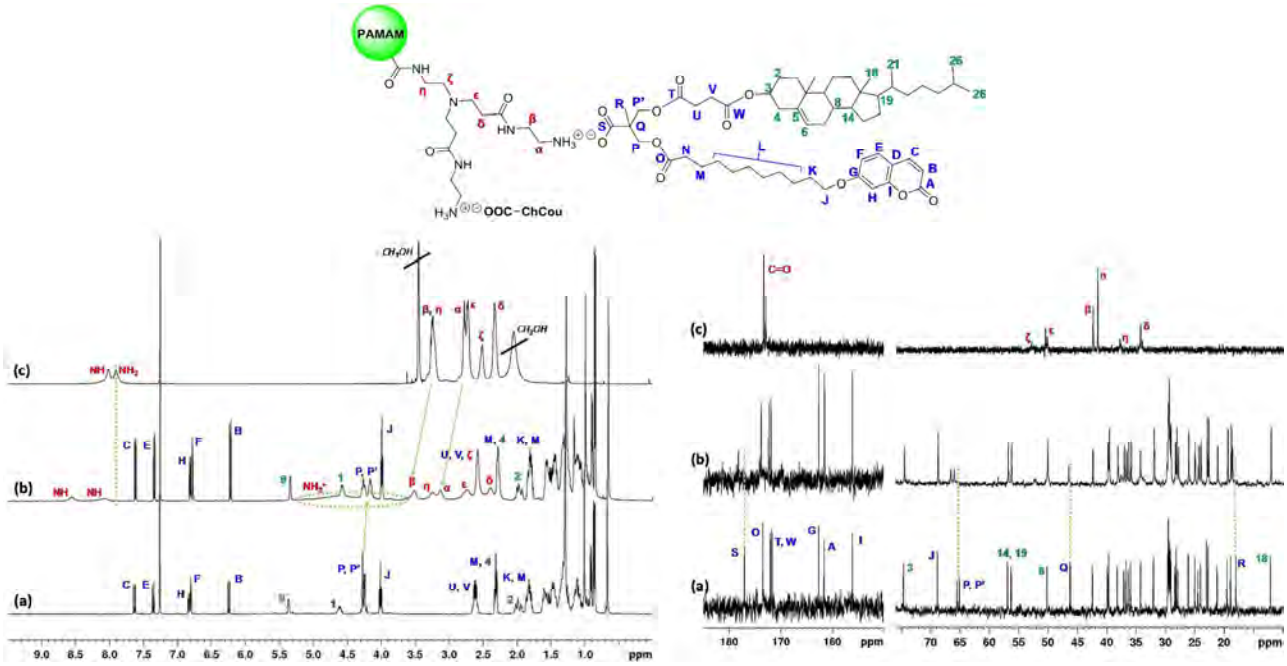

Figure 3. ^{1}H (left) and ^{13}C (right) NMR spectra in $CDCl_3$ solution at 25 °C of: **(a) Ac-ChCou**, **(b)** ionic dendrimer **PAMAM32-ChCou**, and **(c) PAMAM32**.

The ^{1}H NMR spectra recorded in $CDCl_3$ clearly show the formation of the ionic assemblies. As a representative example the ^{1}H NMR spectra of the dendron **Ac-ChCou**, the third generation PAMAM dendrimer (**PAMAM32**) and the ionic dendrimer **PAMAM32-ChCou** complex are shown in **Figure 3**. In the initial dendron, the acid proton signal was very broad and barely visible in the ^{1}H spectrum, thus this signal could not be used to determine the formation of the salt. The protons close to the ionic pairs experienced the highest chemical shifts. For instance, the proton signals of the diastereotopic methylene (H_P and $H_{P'}$) moved to higher field after the formation of the salts. In the same way, quantitative protonation of terminal amine groups of PAMAM dendrimer was confirmed by the absence of the NH_2 proton signal at 7.91 ppm and the appearance of the NH_3^+ broad signal at 5.20-4.00 ppm. The absence of the $CH_2C\underline{H}_2$-NH_2 (H_α, δ= 2.77 ppm) and $C\underline{H}_2CH_2$-NH_2 (H_β, δ= 3.22 ppm) signals and the appearance of the $CH_2C\underline{H}_2$-NH_3^+ (H_α, δ= 3.13 ppm) and $C\underline{H}_2CH_2$-NH_3^+ (H_β, δ= 3.52 ppm) signals, also confirms the quantitative protonation of terminal amine groups.

^{1}H-^{1}H NOESY experiments were also employed to study the formation of these ionic dendrimers in solution. The main feature of NOESY is their ability to provide in a single experiment all the correlations between nuclei which are physically close in space, thus making it a very valuable tool for determining whether supramolecular interactions were established between **Ac-ChCou** dendron and **PAMAM** dendrimer. The ^{1}H-^{1}H NOESY spectrum of **PAMAM32-ChCou** is shown in **Figure S2** (Supporting Information). Significant cross-peaks were observed between the diastereotopic protons of **Ac-ChCou** (H_P and $H_{P'}$) and H_α and H_β protons of the terminal branches of PAMAM, indicating that these groups were close in space because of the ionic pair formation. Besides of this, H_P and $H_{P'}$ docked closely with the terminal NH_3^+ groups of PAMAM.

In the ^{13}C NMR spectra (**Figure 3**) the carboxyl group signal (C_S) of the acid shifts from 176.98 to 178.18, indicating the formation of the carboxylate (COO^-). Likewise, the deprotonation of the carboxylic acid was also corroborated by the displacement of the methylic carbon (C_Q), the methyl (C_R) carbon and the methylene carbons (C_P and $C_{P'}$) to lower field. In addition, when terminal amine groups of PAMAM are protonated, the methylene carbons (C_α and C_β) move from 41.6/42.4 to 39.7/37.7, respectively (data confirmed by ^{1}H-^{13}C HSQC experiments, **Figure S3**).

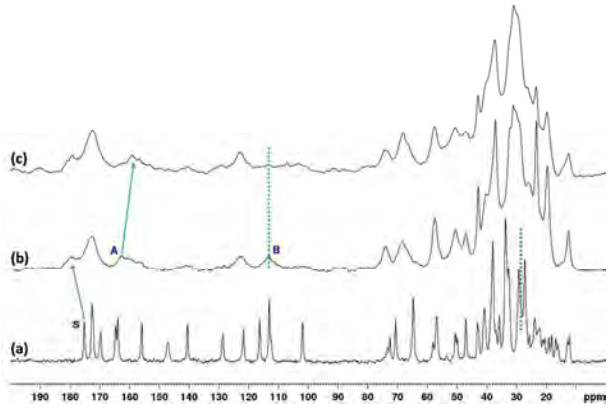

Figure 4. ^{13}C CPMAS NMR spectra of: **(a) Ac-ChCou**, **(b)** ionic dendrimer **PAMAM16-ChCou**, and **(c)** ionic dendrimer **PAMAM16-ChCou** after photodimerization.

View Article Online
DOI: 10.1039/C7TC05009G

Table 1. Thermal properties and structural parameters

	$T_{5\%}$ [a] (°C)	Phase transitions[b]	d_{obs} [c] (Å)	*h k l* [d]	Structural parameters
Ac-ChCou	190	g 9 N 70[e] I	-	-	-
PAMAM4-ChCou	188	g 6 SmA 65[e] I	42.7	1 0 0	d = 42.7 Å
			4.5 (br)		$Ø$ = 14.5 Å
PAMAM8-ChCou	203	g 27 SmA 74 I	43.2	1 0 0	d = 43.3 Å
			21.7	2 0 0	$Ø$ = 20.9 Å
			4.5 (br)		
PAMAM16-ChCou	209	g 21 SmA 63[e] I	46.2	1 0 0	d = 46.2 Å
			23.1	2 0 0	$Ø$ = 28.8 Å
			4.5 (br)		
PAMAM32-ChCou	200	g 18 SmA 75[e] I	41.1	1 0 0	d = 41.1 Å
			4.5 (br)		$Ø$ = 43.5 Å
PAMAM64-ChCou	198	g 29 Col_h 81[e] I	49.3	1 0 0	a = 56.7 Å
			28.2	1 1 0	h_d = 44.0 Å
			4.5 (br)		

[a] Temperature at which 5% mass lost is detected in the thermogravimetric curve. [b] DSC data of the second heating process at a rate of 10 ºC min^{-1}. g: glass, SmA: smectic A mesophase, Col_h: hexagonal columnar mesophase, I: isotropic liquid. [c] *d* value calculated according to Bragg's equation. [d] Miller indices. [e] POM data.

The ^{13}C cross-polarization magic-angle spinning (^{13}C CPMAS) NMR spectra were recorded at room temperature for the ionic hybrid dendrimers (**Figure 4**). The downfield shift of the carboxylic carbon (C_S) signal of **PAMAM16-ChCou** provides strong evidence for the formation of the carboxylate anion.

Thermal properties and mesogenic behavior.

The thermal stability of the ionic dendrimers was studied by thermogravimetric analysis (TGA). All the samples showed good thermal stability and in all cases the 5% weight loss temperature ($T_{5\%}$) was detected at temperatures more than 100°C above the isotropization point (**Table 1**). Thermal transitions and mesomorphic properties were studied by polarized optical microscopy (POM), differential scanning calorimetry (DSC) and X-ray diffraction (XRD). Three cycles were carried out in DSC experiments and data were taken from the second cycle. In some cases, temperatures were taken from POM observations because transition peaks were not detected in DSC curves.

Dendron **Ac-ChCou** displayed a enantiotropic nematic mesophase, which was observed at room temperature by POM on applying mechanical stress to the sample (**Figure S4**). The XRD pattern of the nematic phase contains diffuse scattering at low angles and a diffuse halo at high angles corresponding to the intermolecular short-range interactions between molecules.

All the ionic dendrimers displayed liquid crystalline behavior. The DSC curves showed only a glass transition freezing the mesomorphic order at room temperature. Dendrimers for generations G=0-3 exhibited a smectic A mesophase that was identified by POM on applying mechanical stress to the sample showing birefringent textures (**Figure S4**). However, the G=4 ionic dendrimer **PAMAM64-ChCou**, surrounded by 64 dendrons **Ac-ChCou**, exhibited a hexagonal columnar mesophase. The smectic A and hexagonal columnar nature of the mesophases was confirmed by X-ray diffraction (XRD)

In G=0-3 ionic dendrimers, the XRD patterns were constituted by a diffuse halo in the wide angle region, corresponding to the short-range correlations between the conformationally disordered alkyl chains, and by one or two sharp maxima in the small angle region. These sharp maxima evidence a long-range lamellar packing of molecules, and when there were two low-angle maxima in the reciprocal spacing ratio 1:2, they can be assigned to the first and second order reflections. The layer spacing (*d*) of the SmA mesophase was obtained by applying Bragg's law and they are gathered in **Table 1**.

The XRD pattern obtained for the G=4 ionic dendrimer was consistent with a hexagonal columnar mesophase. It exhibited a diffuse maximum corresponding to a distance of about 4.5 Å between the conformationally disordered aliphatic chains. In the low-angle region the XRD patterns showed a set of two sharp reflections in the reciprocal ratio of 1 : 1/√3. These two reflections can be assigned to the reflections (100) and (110) of a hexagonal columnar arrangement with a lattice parameter (*a*) of 56.7 Å.

On the basis of our previous works on LC dendrimers,[43-44] we propose a cylinder-shaped conformation of the G=0-3 dendrimers, in which the dendrimer matrix occupies the central section whereas the ionic pairs extend up and down with the dendrons statistically distributed (**Figure 5**). To gain

View Article Online
DOI: 10.1039/C7TC05009G

insight into the molecular arrangement and the packing in the mesophase, it is possible to make some theoretical calculations using the experimentally measured spacings (*d*) and the molecular weight values (*M*). The density ρ of a smectic mesophase can be calculated by the formula:[27]

$$\rho = (4 \cdot 10^{24} \cdot M)/(\pi \cdot d \cdot N_A \cdot \emptyset^2)$$

where $\emptyset$ is the diameter of the cylinder and N_A is the Avogadro's number. Assuming that the density of organic compounds is around 1 g·cm^{-3}, it is possible to estimate the diameter $\emptyset$ in Å of the cylindrical dendritic molecules. The results of these calculations show that the diameter of the cylinder increases with increasing the generation of the dendrimer due to the predominant spreading of the dendritic branches of PAMAM in the plane perpendicular to the cylinder axis to accommodate all the dendrons. Indeed, the height of the molecular cylinder (*d*) remains practically constant for all the G=0-3 dendrimers, whereas the cylinder diameter ($\emptyset$) increases from one generation to the next one. This can be explained if the dendritic matrix strongly deforms in the directions parallel to the smectic layers with increasing the generation number. However, the growth of the diameter has a limit where the supermolecule undergoes conformational changes because the cylinder does not have enough space to accommodate the increasingly number of fuctional units. The flexibility of the dendrimer matrix allows a molecular conformation in which the dendrons extend radially from the central dendrimer nucleus (**Figure 5**). The supramolecular organization of these disk-like molecules in columns gives rise to the observed hexagonal columnar mesomorphism. As for the smectic mesophases, simple calculations can be carried out for the columnar mesophases to gain an insight into the packing in the liquid crystal phase. These calculations enable to estimated values for the mean disc thickness (h_d) with the formula:[27]

$$h_d = (20 \cdot M)/(\sqrt{3} \cdot 6.023 \cdot a^2)$$

Comparison of h_d with *a* indicates that the shape of the dendrimer in the mesophase is more appropriately described as a flattened cylinder than a disk. The arrangement of these disks within supramolecular organizations gives rise to cylindrical columns and therefore to the hexagonal columnar mesophase (**Figure 5**).

Polymer network formation by coumarin photodimerization.

The UV-Vis absorption and fluorescence spectra of ionic dendrimers were recorded on dilute solutions (10^{-5} to 10^{-7} M) in tetrahydrofuran (THF) and in thin films at room temperature. The results are given in the Supporting Information. The ionic dendrimers present identical absorption spectra in solid thin film with a band at 323 nm related to the π–π* transition of the coumarin units.

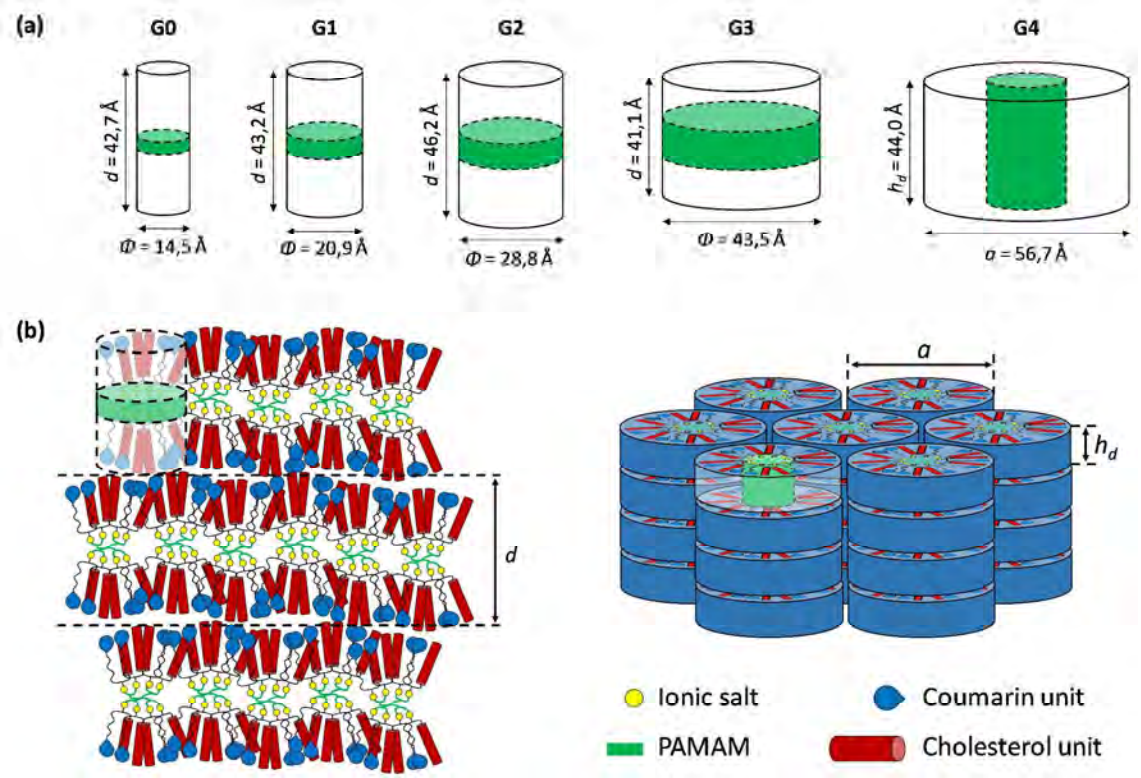

Figure 5. (a) Variation of the elementary ionic dendrimer cylinder as a function of generation number, **(b)** Proposed arrangement of the ionic dendrimers in the smectic A (left) and hexagonal columnar (right) mesophase.

View Article Online
DOI: 10.1039/C7TC05009G

Photodimerization of coumarin units were employed for the crosslinking process by locking the LC arrangement. Exposure of the films to 365 nm UV irradiation caused a decrease of the π–π* band due to photoinduced [2+2] cycloaddition (so-called photodimerization) of the coumarin units (**Figure 6**). After 30 min of light irradiation only slight changes were further detected in the UV-Vis spectra (**Figure 6a**). To examine the structural details of the photo-crosslinking process, irradiated films were studied by FTIR and ^{13}C CPMAS. Irradiation at 365 nm results in coumarin photodimerization as indicated by the decrease the intensity of the C=C stretching band at 1620 cm^{-1} and the shift of the C=O stretching band from 1730 to 1750 cm^{-1} (**Figure 6b**).[45] After photodimerization, 1730 cm^{-1} band did not completely disappear because it comprises contributions from the cholesteryl hemisuccinate ester groups. This reaction can also be followed by ^{13}C CPMAS which showed the disappearance of the peak at 113 ppm (C_B), which corresponds to the C=C moieties (**Figure 4**). Additionally, after coumarin photodimerization the signal at 163 ppm (C_A) is upfield shifted due to the cyclobutane ring formation.[46]

The crosslinking of the smectic or columnar ionic dendrimers gave rise to a LC polymer network, whose lattice spacings are significantly smaller (ca. 5 Å) that those of the starting "single" dendrimer (**Figure 7a**). These results suggest that the ionic pathways have not been disrupted after coumarin photodimerization, thus this reaction can be used to lock in the arrangement of the LC phase (**Figure 7b**)

Proton Conduction Properties

The proton conductivity was measured using electrochemical impedance spectroscopy in samples consisting of films sandwiched between ITO-coated electrodes. The typical impedance response (Nyquist plots) consisted of a suppressed semicircle in the high-frequency region and an incline straight line in the low-frequency range (**Figure S5**).

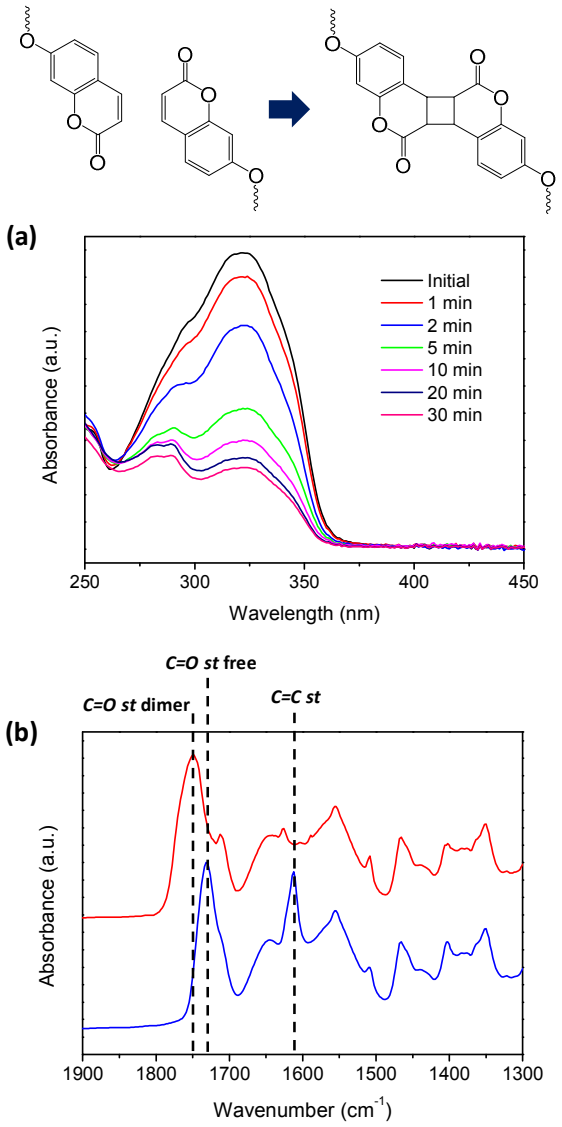

Figure 6. Coumarin photodimerization reaction: **(a)** UV-Vis absorption spectra of a UV-irradiated **PAMAM64-ChCou** film at different times. **(b)** FTIR spectra of **PAMAM16-ChCou** before (blue) and after (red) coumarin photodimerization.

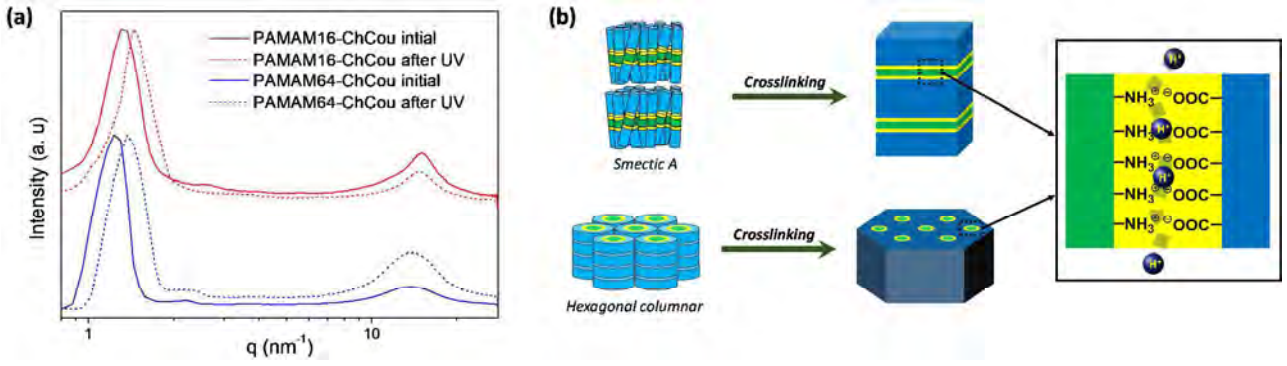

Figure 7 (a) 1D XRD profiles of **PAMAM16-ChCou** and **PAMAM64-ChCou** before and after photodimerization. **(b)** Proton conduction through the nanochannels generated in the ionic dendrimers.

View Article Online
DOI: 10.1039/C7TC05009G

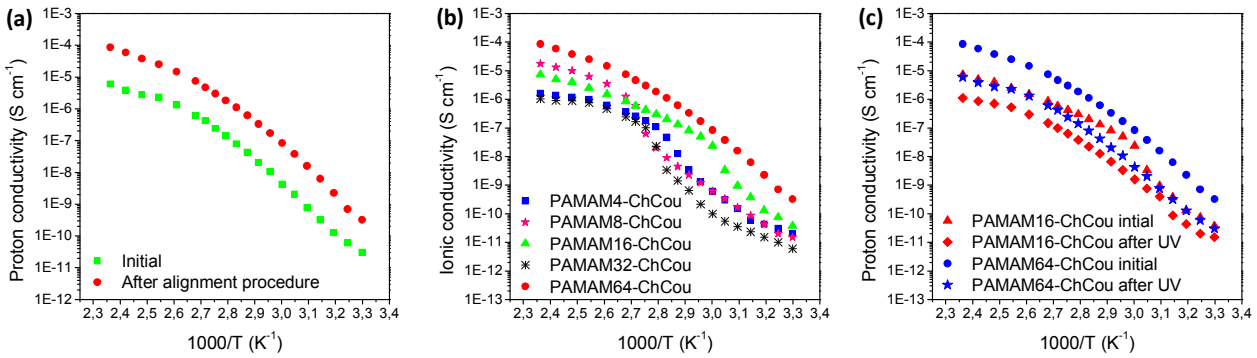

Figure 8. Proton conductivities as a function of the temperature of: **(a) PAMAM64-ChCou**, **(b)** all ionic dendrimers, **(c) PAMAM16-ChCou** and **PAMAM64-ChCou** before and after photodimerization.

Because protons have to travel between two electrodes, in anisotropic materials the measured conductivity depends on the macroscopic degree of order and the orientation of the phase with respect to the electrodes. Initially, a random orientation of the samples (polydomain) was observed between electrodes in just prepared cells. Thus, several alignment procedures (shearing or thermal treatments) were performed in an effort to obtain long-range, uniform planar or homeotropic alignment over large areas of the SmA or Col_h samples, respectively. As a representative example, the proton conductivities of **PAMAM64-ChCou** before and after thermal annealing are shown in **Figure 8a**. The ionic conductivities after annealing are approximately one order of magnitude higher than those of the films without annealing. This result suggests that thermal treatments favors columnar arrangement perpendicular to the electrodes, having a decisive influence in the proton conductivity.

In **Figure 8b**, the proton conductivities (after alignment) were compared among the different generations of the ionic dendrimers. Interestingly, the G=4 ionic dendrimer exhibits the highest conductivity. This result can be understood by keeping in mind that the G=4 dendrimer displayed a hexagonal columnar phase whereas the G=0-3 presented smectic A mesomorphism. Most likely, the supramolecular organization of **PAMAM64-ChCou** may facilitate the protonic charge transport due to the presence of 1D nanochannels. On the other hand, there are no big differences in the ionic conductivities for the G=0-3 ionic dendrimers. Therefore, these results suggest that the hexagonal columnar organization in the liquid crystal state clearly favors proton conduction.

The proton conductivities after coumarin photodimerization were estimated by taking compounds **PAMAM64-ChCou**, which exhibits a hexagonal columnar mesophase, and **PAMAM16-ChCou**, with a smectic A mesophase, as representative examples (**Figure 8c**). It is remarkable that after crosslinking both dendrimers showed a decrease in conductivities similar to the previously reported polymerizable liquid crystals whose conductivities reduced about one-order of magnitude after polymerization due to the decrease in the mobility of ionic moieties.[21-22]

Conclusions

A new strategy for the preparation proton conductive materials has been developed using ionic LC dendrimers combined with a crosslinking reaction based on coumarin photodimerization. 1D and 2D ionic nanosegregated assemblies can be obtained in a modular approach using different generation dendrimers. The use of coumarin photodimerization impart a new tool to fabricate mechanical stable ionic materials. All ionic materials showed good proton conductivity and it is expected that macroscopic alignment will enhance this. The proton conduction in these ionic LC dendrimers may open a new path in the search of electrolyte materials for the preparation of electrochemical devices.

Acknowledgements

This work was supported by the MINECO-FEDER funds (project CTQ2015-70174 and PhD grant to A. Concellón), Gobierno de Aragón-FSE (Research Group E04). Ting Liang is financially supported by the China Scholarship Council (CSC). Authors would like to acknowledge the use of the SAI (UZ) and CEQMA (UZ-CSIC) Services. A. Concellón thanks M. Pilz da Cunha for her assistance with de X-ray diffraction.

Notes and references

1. M. Yoshio, T. Kato, in *Handbook of Liquid Crystals*, Vol. 8 (Eds: J. W. Goodby, P. J. Collings, T. Kato, C. Tschierske, H. Gleeson, P. Raynes), Wiley-VCH Verlag GmbH & Co. KGaA, 2014, 727.
2. A. Martínez-Felipe, *Liq. Cryst.* 2011, **38**, 1607.
3. W. Pisula, M. Zorn, J. Y. Chang, K. Müllen, R. Zentel, *Macromol. Rapid Commun.* 2009, **30**, 1179.
4. M. O'Neill, S. M. Kelly, *Adv. Mater.* 2011, **23**, 566.
5. E.-K. Fleischmann, R. Zentel, *Angew. Chem. Int. Ed.* 2013, **52**, 8810.
6. T. Kato, M. Yoshio, T. Ichikawa, B. Soberats, H. Ohno, M. Funahashi, *Nat. Rev. Mater.* 2017, **2**, 17001.
7. T. Kato, N. Mizoshita, K. Kishimoto, *Angew. Chem. Int. Ed.* 2006, **45**, 38.
8. T. Kato, *Science* 2002, **295**, 2414.

View Article Online
DOI: 10.1039/C7TC05009G

9. R. L. Kerr, S. A. Miller, R. K. Shoemaker, B. J. Elliott, D. L. Gin, *J. Am. Chem. Soc.* 2009, **131**, 15972.
10. T. Kato, *Angew. Chem. Int. Ed.* 2010, **49**, 7847.
11. D. Basak, S. Christensen, S. K. Surampudi, C. Versek, D. T. Toscano, M. T. Tuominen, R. C. Hayward, D. Venkataraman, *Chem. Commun.* 2011, **47**, 5566.
12. R. D. Costa, F. Werner, X. Wang, P. Grönninger, S. Feihl, F. T. U. Kohler, P. Wasserscheid, S. Hibler, R. Beranek, K. Meyer, D. M. Guldi, *Advanced Energy Materials* 2013, **3**, 657.
13. B. Soberats, M. Yoshio, T. Ichikawa, S. Taguchi, H. Ohno, T. Kato, *J. Am. Chem. Soc.* 2013, **135**, 15286.
14. D. Högberg, B. Soberats, S. Uchida, M. Yoshio, L. Kloo, H. Segawa, T. Kato, *Chem. Mater.* 2014, **26**, 6496.
15. E. Tunkara, C. Albayrak, E. O. Polat, C. Kocabas, Ö. Dag, *ACS Nano* 2014, **8**, 11007.
16. C. Cuerva, J. A. Campo, M. Cano, J. Sanz, I. Sobrados, V. Diez-Gómez, A. Rivera-Calzada, R. Schmidt, *Inorg. Chem.* 2016, **55**, 6995.
17. J. H. Lee, K. S. Han, J. S. Lee, A. S. Lee, S. K. Park, S. Y. Hong, J.-C. Lee, K. T. Mueller, S. M. Hong, C. M. Koo, *Adv. Mater.* 2016, **28**, 9301.
18. D. Högberg, B. Soberats, M. Yoshio, Y. Mizumura, S. Uchida, L. Kloo, H. Segawa, T. Kato, *ChemPlusChem* 2017, **82**, 834.
19. X. Feng, S. Nejati, M. G. Cowan, M. E. Tousley, B. R. Wiesenauer, R. D. Noble, M. Elimelech, D. L. Gin, C. O. Osuji, *ACS Nano* 2016, **10**, 150.
20. A. Yamashita, M. Yoshio, S. Shimizu, T. Ichikawa, H. Ohno, T. Kato, *J. Polym. Sci. Part A: Polym. Chem.* 2015, **53**, 366.
21. K. Kishimoto, M. Yoshio, T. Mukai, M. Yoshizawa, H. Ohno, T. Kato, *J. Am. Chem. Soc.* 2003, **125**, 3196.
22. M. Yoshio, T. Kagata, K. Hoshino, T. Mukai, H. Ohno, T. Kato, *J. Am. Chem. Soc.* 2006, **128**, 5570.
23. T. Liang, H. P. C. van Kuringen, D. J. Mulder, S. Tan, Y. Wu, Z. Borneman, K. Nijmeijer, A. P. H. J. Schenning, *ACS Applied Materials & Interfaces* 2017, **9**, 35218.
24. S. Hernández-Ainsa, M. Marcos, J. L. Serrano, in *Handbook of Liquid Crystals*, Vol. 7 (Eds: J. W. Goodby, P. J. Collings, T. Kato, C. Tschierske, H. Gleeson, P. Raynes), Wiley-VCH Verlag GmbH & Co. KGaA, 2014, 259.
25. B. M. Rosen, C. J. Wilson, D. A. Wilson, M. Peterca, M. R. Imam, V. Percec, *Chem. Rev.* 2009, **109**, 6275.
26. M. Marcos, R. Martín-Rapún, A. Omenat, J. Barberá, J. L. Serrano, *Chem. Mater.* 2006, **18**, 1206.
27. R. Martín-Rapún, M. Marcos, A. Omenat, J. Barberá, P. Romero, J. L. Serrano, *J. Am. Chem. Soc.* 2005, **127**, 7397.
28. S. Hernández-Ainsa, M. Marcos, J. Barberá, J. L. Serrano, *Angew. Chem. Int. Ed.* 2010, **49**, 1990.
29. S. Hernández-Ainsa, J. Barberá, M. Marcos, J. L. Serrano, *Chem. Mater.* 2010, **22**, 4762.
30. S. Castelar, P. Romero, J. L. Serrano, J. Barbera, M. Marcos, *RSC Adv.* 2015, **5**, 65932.
31. G. M. Bögels, H. P. C. van Kuringen, I. K. Shishmanova, I. K. Voets, A. P. H. J. Schenning, R. P. Sijbesma, *Advanced Materials Interfaces* 2015, **2**, 1500022.
32. D. A. Tomalia, J. M. J. Fréchet, in *Dendrimers and Other Dendritic Polymers*, John Wiley & Sons, Ltd, 2002.
33. G. R. Newkome, C. N. Moorefield, F. Vögtle, in *Dendrimers and Dendrons*, Wiley-VCH Verlag GmbH & Co. KGaA, 2004.
34. F. Vögtle, G. Richardt, N. Werner, in *Dendrimer Chemistry*, Wiley-VCH Verlag GmbH & Co. KGaA, 2009.
35. D. Astruc, E. Boisselier, C. Ornelas, *Chem. Rev.* 2010, **110**, 1857.
36. S. R. Trenor, A. R. Shultz, B. J. Love, T. E. Long, *Chem. Rev.* 2004, **104**, 3059.
37. X. Ren, M. E. Kondakova, D. J. Giesen, M. Rajeswaran, M. Madaras, W. C. Lenhart, *Inorg. Chem.* 2010, **49**, 1301.
38. C. Bazzicalupi, C. Caltagirone, Z. Cao, Q. Chen, C. Di Natale, A. Garau, V. Lippolis, L. Lvova, H. Liu, I. Lundström, M. C. Mostallino, M. Nieddu, R. Paolesse, L. Prodi, M. Sgarzi, N. Zaccheroni, *Chem. Eur. J.* 2013, **19**, 14639.
39. A. Gaspar, M. J. Matos, J. Garrido, E. Uriarte, F. Borges, *Chem. Rev.* 2014, **114**, 4960.
40. P. Kotchapradist, N. Prachumrak, T. Sunonnam, R. Tarsang, S. Namuangruk, T. Sudyoadsuk, T. Keawin, S. Jungsuttiwong, V. Promarak, *Dyes Pigm.* 2015, **112**, 227.
41. A. Concellón, M. Bucoş, J. L. Serrano, P. Romero, M. Marcos, *RSC Adv.* 2016, **6**, 65179.
42. A. Concellón, M. Marcos, P. Romero, J. L. Serrano, R. Termine, A. Golemme, *Angew. Chem. Int. Ed.* 2017, **56**, 1259.
43. M. Marcos, R. Martin-Rapun, A. Omenat, J. L. Serrano, *Chem. Soc. Rev.* 2007, **36**, 1889.
44. J. Barbera, B. Donnio, L. Gehringer, D. Guillon, M. Marcos, A. Omenat, J. L. Serrano, *J. Mater. Chem.* 2005, **15**, 4093.
45. A. Trajkovska, C. Kim, K. L. Marshall, T. H. Mourey, S. H. Chen, *Macromolecules* 2006, **39**, 6983.
46. M. V. S. N. Maddipatla, D. Wehrung, C. Tang, W. Fan, M. O. Oyewumi, T. Miyoshi, A. Joy, *Macromolecules* 2013, **46**, 5133.

View Article Online
DOI: 10.1039/C7TC05009G

GRAPHICAL ABSTRACT

Proton-conductive materials formed by coumarin photocrosslinked ionic liquid crystal dendrimers

Alberto Concellón, Ting Liang, Albertus P. H. J. Schenning, José Luis Serrano, Pilar Romero, and Mercedes Marcos**

We have successfully developed a new strategy for the preparation proton conductive materials using ionic LC dendrimers combined with a crosslinking reaction based on coumarin photodimerization.